This is a repository copy of *Highly effective Cs+ removal by turbidity-free potassium copper hexacyanoferrate-immobilized magnetic hydrogels*.

Accepted Manuscript

Title: Highly effective Cs$^+$ removal by turbidity-free potassium copper hexacyanoferrate-immobilized magnetic hydrogels

Authors: Yun Kon Kim, Taegeon Kim, Yonghwan Kim, David Harbottle, Jae W. Lee

Please cite this article as: Yun Kon Kim, Taegeon Kim, Yonghwan Kim, David Harbottle, Jae W.Lee, Highly effective Cs+ removal by turbidity-free potassium copper hexacyanoferrate-immobilized magnetic hydrogels, Journal of Hazardous Materialshttp://dx.doi.org/10.1016/j.jhazmat.2017.06.066

Highly effective Cs+ removal by turbidity-free potassium copper hexacyanoferrate-immobilized magnetic hydrogels

Yun Kon Kim[a,‖], Taegeon Kim [a,‖], Yonghwan Kim[a], David Harbottle[b] and Jae W. Lee[a,*]

[a]Department of Chemical and Biomolecular Engineering, Korea Advanced Institute of Science and Technology (KAIST), Daejeon 305-701, Republic of Korea

[b]School of Chemical and Process Engineering, University of Leeds, Leeds LS2 9JT, United Kingdom

[‖] These authors contributed equally to this work

*To whom correspondence should be addressed: jaewlee@kaist.ac.kr

1

Graphical Abstract
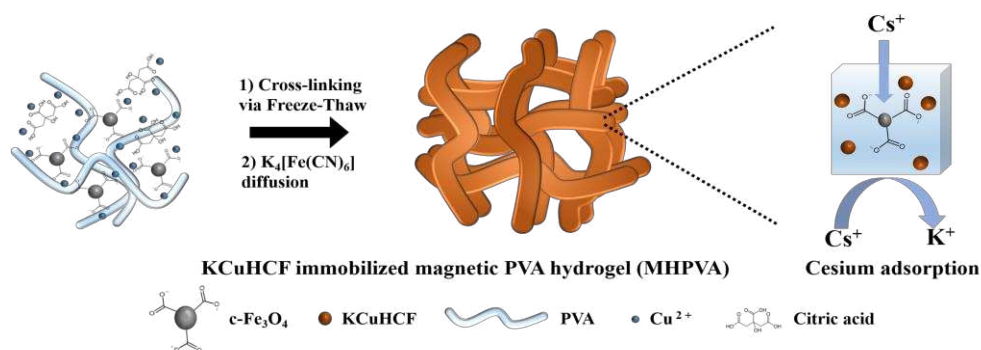
Highlights

- ✓ The magnetic hydrogel (MHPVA) was prepared via a facile freeze/thaw method.
- ✓ The MHPVA has a good Cs^+ adsorption capacity of 82.8 mg/g.
- ✓ It exhibits very high removal efficiency of 99.9% in 8.3 ppm Cs^+ solution.
- ✓ It shows high Cs^+ selectivity even in the presence of various competing cations.
- ✓ It can be rapidly recovered from wastewater by a magnet without any turbidity.

Abstract

Potassium copper hexacyanoferrate-immobilized magnetic hydrogel (MHPVA) has been synthesized via a facile freeze/thaw crosslinking method. The citric acid coated Fe_3O_4 is embedded into the hydrogel matrix to facilitate the dispersion of nano-sized KCuHCF particles for Cs^+ removal, followed by the rapid recovery of the composite in a magnetic field. The Cs^+ adsorption behavior of the MHPVA is fitted well with the Langmuir isotherm and the pseudo-second-order kinetic model. The MHPVA exhibits both high Cs^+ adsorption capacity (82.8 mg/g) and distribution coefficient (K_d) of 1.18×10^6 mL/g (8.3 ppm Cs^+, V/m = 1000 mL/g). Sorption of above 90% Cs^+ to the MHPVA is achieved in less than 3 h of contact time.

Moreover, the MHPVA reveals stable and high Cs^+ removal efficiency across a wide pH range from 4 to 10. In terms of Cs^+ selectivity, the MHPVA shows above 96% removal efficiency in the presence of 0.01 M competing cations such as Mg^{2+}, Ca^{2+}, Na^+, and K^+ with 1 ppm of Cs^+. From a practical perspective, the MHPVA still exhibits stable and promising selective properties even in groundwater and seawater conditions and after 5 days of contact time the used adsorbent is rapidly recovered leaving a turbidity-free aqueous environment.

1. Introduction

Nuclear power is seen as a viable option to meet future energy demands and alleviate the ever growing concerns of global warming. At present nuclear power accounts for about 9.7 % of the world's energy [1], although this percentage is anticipated to increase. However, nuclear energy can also pose environmental concerns [2] with legacy waste and accidental release of radionuclides through incident, such as that witnessed at Chernobyl (1986) and Fukushima (2011), threatening ecosystems and human lives [3].

Radioactive wastes consist of various radioactive isotopes including monovalent, divalent, and trivalent metal cations [4]. Among the radionuclides, radioactive cesium-137 (^{137}Cs) is a strong gamma emitter, which has been identified as a problematic radionuclide due to its long half-life of 30.1 years, and serious radiological hazard to the environment and human [5]. Although there are a variety of effective materials to remove trace amounts of

3

multivalent radioactive isotopes today, the removal of monovalent cesium ions remains a challenge [4]. The most effective method for the removal of Cs^+ is utilizing adsorption or ion-exchange media [6].

Various types of cesium adsorbents such as zeolites [7, 8], silicotitanates [9-11], chalocogenides [12-14], and clay minerals [5, 15], have been studied previously, but all of these adsorbents are low in selectivity or difficult to scale up for practical application. As an alternative, transition metal hexacyanoferrates (HCFs) have been proposed as highly selective adsorbents for Cs^+, with the synthesis methods considered relatively simple and low-cost [3, 16-19]. HCF has a perovskite-like face centered cubic structure with a channel diameter of around 0.32 nm, which is well fitted with a small hydrated ion such as Cs^+ [20]. In particular, it has been reported that the copper based HCF has high Cs^+ sorption capacity and chemical stability [21-23]. These advantageous properties have led to a great deal of interest in utilizing copper based HCF as a superior adsorbent for the selective removal of Cs^+ from radioactive contaminated environments. However, the ultra-fine particle size of the bulk HCF materials hinders their direct application in batch or continuous processes due to issues associated with containment and separation of the fine particles [24].

Magnetic separation, mainly using Fe_3O_4 nanoparticles, is a facile method to recover adsorbent from wastewater, and has been used for the treatment of heavy metal and organic pollutants. Many researchers have devised methods to combine HCFs and Fe_3O_4 nanoparticles for the integrated process of effective Cs^+ removal and rapid separation [25-27]. Yang et al. has reported in situ synthesis of magnetic Prussian blue/graphene oxide

4

nanocomposites [28], as well as alginate encapsulated particles [1], which exhibited maximum adsorption capacities of 55.56 mg/g and 43.52 mg/g, respectively. Change et al. fabricated magnetic Prussian blue core/shell nanoparticles to improve the leaching stability of Prussian blue particles [29]. Although these studies demonstrated promising technologies, there remain some disadvantages in terms of low availability of active sites due to the aggregation of nanoparticles, and turbidity of the aqueous environment related to incomplete recovery of the fine-powder magnetic adsorbent.

In the current study, potassium copper HCF (KCuHCF) and Fe_3O_4 immobilized Poly(vinyl alcohol) (PVA) magnetic hydrogel adsorbent (MHPVA) was successfully synthesized via a facile two step method (Fig.1). PVA was used as a hydrogel backbone, which has abundant hydroxyl groups coordinating metal ions [30]. Moreover, citric acid functionalized Fe_3O_4 (c-Fe_3O_4) was used to prevent particle aggregation and to improve the dispersion of KCuHCF nanoparticles. In the first step, Cu^{2+} ions and c-Fe_3O_4 dispersed hydrogel film was produced by a freeze-thaw crosslinking method. Next, $K_4[Fe(CN)_6]$ was diffused into the prepared film structure, leading to the formation of KCuHCF within the hydrogel. The chemical and physical characteristics of the synthesized adsorbents were determined using various analytical techniques. In terms of the Cs^+ adsorption behavior, the MHPVA exhibited maximum capacities of 82.8 mg/g and high selectivity for Cs^+ even when dispersed in excess amounts of competing cations. Furthermore, in a magnetic field, the spent adsorbent was easily recovered from the waste solution without any turbidity and missing particles.

5

2 Experimental

Materials, synthesis of citric acid coated Fe_3O_4 (c-Fe_3O_4), PVA-gel, KCuHCF-immobilized non-magnetic PVA hydrogel (HPVA), and bulk KCuHCF, and characterization are provided in the Supplementary Material.

2.1 Synthesis of MHPVA

First, 1 g of PVA was dissolved in 7 mL deionized water at 80 °C for 1 h under constant stirring. Separately, 0.39 g of $CuSO_4$ was dissolved in 3 mL deionized water. Also, 0.6 g of citric acid was added to the $CuSO_4$ solution to assist distribution of Cu^{2+} ions, with the solution stirred at room temperature for 30 min. After that, 0.25 g of the prepared c-Fe_3O_4 nanoparticles was mixed with the $CuSO_4$ solution. The mixture was poured into the prepared PVA solution and vigorously stirred for 30 min at 30 °C. Then, the homogeneous solution was cast onto a teflon dish, and rapidly frozen at a temperature of -20 °C for 1 h. The frozen solution was thawed at 25 °C in an oven for 1 h. After the freeze-thaw cycle was repeated 3 times, the crosslinked PVA hydrogel film was obtained. The formed film was submerged into the mixture of 100 mL $K_4[Fe(CN)_6]$ (0.1 M) and 200 mL acetone, and continuously stirred for 24 h at 20 °C.

Acetone was used as a non-solvent to suppress the reverse diffusion of the embedded Cu^{2+} from the film structure into the liquid phase. As the low-boiling acetone was evaporated, the solubility of $K_4[Fe(CN)_6]$ gradually increased in the water-rich phase and diffused into the hydrogel to react with Cu^{2+}. Hence, KCuHCF nanoparticles were formed in the interior of the film. Our previous research reported the effect of acetone to enhance the retention of

6

KCuHCF nanoparticles in the hydrogel structure by inhibiting the reverse diffusion of Cu^{2+} [23]. Finally, the synthesized MHPVA was thoroughly washed with DI water to eliminate the citric acid and residual impurities, followed by drying the MHPVA in an oven at 30 °C for 24 h.

2.2 Cesium adsorption

The simulated radioactive waste water solution containing Cs^+ was prepared by dissolving cesium chloride in deionized (DI) water. Cesium adsorption experiments were performed using batch-shaking method with V/m = 1000 mL/g of solution volume per adsorbent mass ratio. The mixture was shaken (200 rpm) for 24 h at 25 °C. After adsorption, the liquid phase was separated using syringe filters (0.45 μm) and the equilibrium Cs^+ concentration was determined in triplicate with an inductively coupled plasma mass spectrometer (ICP-MS 7700S, Agilent) and the average value was reported. The adsorption capacity (q_e, mg/g), distribution coefficient (K_d, mL/g), and removal efficiency (RE, %) were calculated as follows:

$$q_e = (C_0 - C_e) \times V/m \qquad\qquad (1)$$

$$K_d = (C_0 - C_e)/C_e \times V/m \qquad\qquad (2)$$

$$RE = (C_0 - C_t)/C_0 \times 100 \qquad\qquad (3)$$

Here C_0 and C_e are the initial and equilibrium concentrations of Cs^+ (mg/L) in solution, C_t represents the Cs^+ concentration (mg/L) in the sampled liquid phase at specified time intervals, m represents the mass of the adsorbent (g), and V is the total volume of the solution (L).

3 Results and discussion

3.1 Microscopic characterization

The internal porous structures of the prepared hydrogels were investigated by SEM. All samples were immersed in DI water for 24 h and freeze-dried at -50 °C before SEM analysis. The PVA-gel (Fig. 2a) shows the internal macro-porous 3D-structure which consists of the crosslinked PVA polymer chain. After incorporating KCuHCF and c-Fe_3O_4 in the hydrogel structure (Fig.2b), while less porous, a thicker and more rigid wall structure was formed. At higher magnification, Fig. 2c shows a roughened surface indicating the confinement of nanoparticles in the polymer structure. The distribution of KCuHCF particles was supported by the elemental mapping analysis of the MHPVA, shown in Fig. S1. The elemental mapping images clearly indicate the dispersion of elements such as Fe, Cu, N, and K associated with KCuHCF and c-Fe_3O_4 within the whole polymer structure.

The difference between the HPVA and MHPVA structures was investigated using TEM. Fig. 2d confirms the presence of nanoparticles in the HPVA, although not clearly distinguished by the thick polymer backbone. On the other hand, the MHPVA (Fig. 2e) shows additional dark spots, indicative of the nanoparticles which are similar to those observed in the TEM image of the synthesized bulk c-Fe_3O_4 (Fig. S2). Moreover, the high resolution-TEM image (Fig. 2f) confirms the existence of nanoparticles of different shape and lattice distances. The square- and circular-like nanocrystallites have lattice distances of 0.50 nm and 0.25 nm, respectively, which correspond to d-spacings of the (200) and (311) direction for

8

KCuHCF and Fe_3O_4, respectively [31, 32]. Thus, the 3D-interconnected hydrogel structure and immobilized nanoparticles were clearly identified by electron microscopy techniques.

3.2 Chemical characterization

Fig. 3 depicts the XRD patterns of the prepared samples. The PVA-gel, HPVA, and MHPVA indicate PVA characteristic peaks centered at 19.4° and 22.9°. The obtained bulk KCuHCF shows strong peaks around 17.7° (200), 25° (220), 36° (400), 40° (420), 44° (422), 52° (440), 55° (600) and 58° (620), which correspond to those of the $K_2Cu[Fe(CN)_6]$ (PDF no. 01-075-0023). The XRD patterns for the KCuHCF immobilized HPVA and MHPVA were also in good agreement with the reference of $K_2Cu[Fe(CN)_6]$. Compared with the HPVA, the MHPVA represents Fe_3O_4 related peaks around 30° and 63° [32]. Two-theta values around 35°, 43°, and 57° are not clearly distinguished due to overlap with the peaks of KCuHCF, but the higher intensity at 35° supports the presence of Fe_3O_4 nanoparticles. Therefore, the XRD patterns demonstrate the co-immobilization of KCuHCF and Fe_3O_4 nanoparticles in the synthesized MHPVA structure.

Furthermore, the crystalline size of the KCuHCF and $c-Fe_3O_4$ in the MHPVA was calculated using Scherrer's equation [17]:

$$L = \frac{K \cdot \lambda}{\beta \cdot \cos \theta} \qquad (4)$$

where K is a dimensionless shape factor varying with the actual shape of the crystallite (taken as 0.94), λ is the X-ray wavelength (nm), β is the line broadening at half maximum intensity

(FWHM, rad), and θ is the diffraction angle at the specified peak (rad). The calculated average particle sizes from the peaks at 25° and 30° were equal to ~12 nm and ~7 nm which are slightly smaller but consistent with the TEM result, considering the aggregation of nanoparticles [33, 34].

As shown in Fig.4, the FTIR spectra for the bulk KCuHCF show the characteristic peaks of C≡N stretching vibration (2070 cm^{-1}), Fe-CN deformation (580 cm^{-1}) and Cu-CN stretching mode (470 cm^{-1}) [35, 36]. The prepared PVA-gel exhibits broad bands between 3000 cm^{-1} and 3500 cm^{-1} indicative of -OH stretching vibrations [37], and the peak around 2900 cm^{-1} is assigned to C-H stretching vibrations from the PVA polymer backbone [38]. These chemical properties which are related to both bulk KCuHCF and PVA are also represented in the FTIR data for the HPVA and MHPVA, confirming the successful synthesis of the crosslinked polymer and nanoparticle composite. The c-Fe$_3$O$_4$ showed a sharp peak at 590 cm^{-1} attributed to Fe-O bond. The strong band at 1520 cm^{-1} and 1413 cm^{-1}, which are assigned to the asymmetric and symmetric COO$^-$ stretching vibration, respectively, demonstrates the incorporation of citric acid with Fe$_3$O$_4$ [32]. As the IR results for the c-Fe$_3$O$_4$, the distinct sharp peak at 595 cm^{-1} in the MHPVA supports the immobilization of magnetic nanoparticles.

XPS measurements provide detailed information about chemical bonds and Fe oxidation states. The peaks in the survey spectrum (Fig. 5a) reveal the presence of Cu, Fe, O, N, C, and K elements in the MHPVA. In the C1s deconvolution spectra (Fig. 5b), four different peaks centered at 284.7, 286.1, 285.7 and 288.3 eV were identified corresponding to

C-C, C-O in PVA, C≡N in the KCuHCF and O=C-O in the c-Fe_3O_4, respectively [28]. The

deconvoluted Fe2p core level spectra (Fig. 5c) represent two different oxidation states Fe^{2+}

(708.1 and 722.5 eV) and Fe^{3+} (711.1 and 724.8 eV) [39, 40]. Compared with the XPS

spectra of the bulk KCuHCF (Fig 5d), the high intense Fe^{3+} peaks are related to the

incorporated c-Fe_3O_4. Although the small shoulder at around 724 eV and 710 eV in the Fe

spectra of bulk KCuHCF indicate the partial oxidation of Fe^{2+}, the results confirm that most

of the Fe in KCuHCF particles was present in the form of Fe^{2+} valence state.

3.3 Textural characterization

The chemical compositions of the HPVA and MHPVA were precisely measured using

ICP-OES analysis. The measured and calculated values are listed in Table 1. Recognizing the

XRD patterns ($K_2Cu[Fe(CN)_6]$) and Fe^{2+} valence state in the XPS spectra, the stoichiometric

chemical composition of the KCuHCF was set as $K_{4x-2}Cu[Fe(CN)_6]_x$ [17, 23]. Based on the

measured amount of Cu, K/Cu was determined and subsequently Fe in HCF/Cu was

calculated by the stoichiometric charge balance. The MHPVA (19.5 wt %) and HPVA (20.1

wt %) indicate comparable KCuHCF wt %, but the chemical compositions are noticeably

different. The difference may be derived from the addition of c-Fe_3O_4, because the other

components and experimental conditions were identical in the preparation step for both the

MHPVA and HPVA. The distributed c-Fe_3O_4 contributes to make additional space between

the polymer chains along with the stabilization of Cu^{2+} ions with the aid of the coated citric

acid functionalities. This is supported by the higher Fe(HCF)/Cu ratio in the MHPVA. In the

case of the HPVA, the amount of Cu was higher than Fe by 1.6 times. However, for the

MHPVA, the ratio of Cu to Fe was about 1.2 indicating more efficient distribution of Cu^{2+}

11

ions throughout the polymer matrix. The higher K^+ content in the MHPVA can be also explained, considering that the higher negative charge induced by the charge difference between Cu^{2+} and $[Fe(CN)_6]^{4-}$ (smaller Cu to Fe ratio) should be compensated by the higher amount of K^+.

The thermal stability was investigated by the thermogravimetric analysis (TGA) under N_2 atmosphere. For c-Fe_3O_4 (Fig. S3), the initial weight loss of ~ 4 % up to 160 °C was related to the elimination of free and interstitial water molecules. Additional weight loss (~10 %) up to 570 °C was associated with the decomposition of the functionalized citric acid. In the case of the PVA-gel, HPVA, and MHPVA (Fig. 6), initial weight loss up to 220 °C was associated to the evaporation of adsorbed water. The rapid weight loss in the temperature range of 220 to 500 °C was ascribed to the degradation of PVA backbone and removal of oxygen functional groups [41]. Beyond 330°C, the gradual weight loss for the HPVA and MHPVA was due to the decomposition of both the PVA hydrogel and hydrogen cyanide from the KCuHCF structure [31, 42]. At 600 °C, the mass difference between the PVA-gel and HPVA was equal to 19.3 %, which is comparable to the calculated KCuHCF content (20.1 %) determined from the ICP-OES analysis. In the case of the MHPVA, the residual weight was 37 %, which is about 15 % higher than that of the HPVA and this 15 % difference was mainly associated with the Fe_3O_4 content in the MHPVA.

3.4 Magnetic property

Fig. 7a shows the magnetic hysteresis curve measured at room temperature with a

vibrating sample magnetometer (VSM). The data indicates that the HPVA has no magnetization, but the MHPVA exhibits obvious magnetic hysteresis. The saturation magnetization and the coercive force for the MHPVA were 6 emu/g and 896 Oe, respectively, indicating sufficient magnetic properties for the facile recovery of the used adsorbent. The evaluation for the magnetic separation was conducted by immersing 0.2 g of the MHPVA in 200 mL of DI water and placing a magnet on the wall of the glass bottle. Sample immersion lasted for 5 days with continuous shaking, and 1 mL aliquots were removed at specific times for the ICP-MS analysis to confirm the release behavior of c-Fe_3O_4 and KCuHCF particles. From Table 2 and Fig. 7b, it is apparent that even after 5 days, the amount of Fe and Cu released from the MHPVA was very small, below 0.073 and 0.022 ppm, respectively, and the solution remained visually transparent. Moreover the MHPVA was immediately attracted by the magnet and there was no turbidity by the residue, demonstrating a potential application for a very fast and complete separation of the MHPVA after the removal of Cs^+ from contaminated environments.

3.5 Adsorption isotherms and kinetics

The equilibrium adsorption amounts were measured by increasing the initial concentrations of Cs^+. For both the HPVA and MHPVA (Fig. 8), initially, the isotherms show a rapid increase of Cs^+ uptake due to the abundant adsorption sites, but the rate of uptake gradually decreased and finally plateaued towards the saturation capacity. To evaluate thermodynamic parameters of the HPVA and MHPVA, two adsorption isotherm models, Langmuir and Freundlich, were introduced. The Langmuir model assumes equivalent and independent adsorption sites, so it reveals uniform monolayer adsorption of Cs^+. The

13

nonlinear form of Langmuir equation is defined as:

$$Q = \frac{Q_m b C_e}{1 + b C_e} \qquad (5)$$

where Q is the adsorbed amount of Cs^+ per unit weight of adsorbent (mg/g) and C_e is the

equilibrium concentration of Cs^+ in aqueous phase (mg/L). Q_m and b are saturation uptake

(mg/g) and the affinity coefficient (L/mg), respectively. Whereas, the Freundlich isotherm is

an empirical model indicating multilayer adsorption with heterogeneous surface energy. The

equation is defined as follows:

$$Q = K_F C_e^{1/n} \qquad (6)$$

where K_F (L/mg) and n are Freundlich constants reflecting adsorption loading and intensity of

adsorption.

All the related parameters and correlation constants (R^2) are listed in Table 3. Both

the HPVA and MHPVA indicate higher correlation constants ($R^2 = 0.95$) for the Langmuir

isotherm compared to the Freundlich isotherm. Moreover, Freundlich constant n is much

greater than 1, indicating that the adsorbed amount is constant regardless of the Cs^+

equilibrium concentration. This characteristic is well matched to the behavior of the

experimental data and suggests that the adsorption mechanism is mainly by monolayer

coverage of the Cs^+ adsorbate [43]. Comparing the saturation uptake of Q_m, the MHPVA has

about 1.3 times higher capacity than that of the HPVA. The increased performance is related

to the higher K^+ content in the MHPVA (Table 1), as reported in previous studies [3, 17, 23,

44]. The adsorption capacity of the MHPVA matched the previous results for magnetic based

Cs$^+$ adsorbent (Table 4). Such good comparison demonstrates that the MHPVA is an effective

Cs$^+$ adsorbent in terms of not only facile and fast magnetic separation, but also adsorption

capacity.

Adsorption kinetics was studied to determine the usefulness of the adsorbents to

remove a low concentration of Cs$^+$ ($\approx$ 8 ppm) from contaminated water. For the kinetic

experiments, 0.2 g of the adsorbent was immersed in 200 mL of Cs$^+$ solution, and 1 mL

aliquots were sampled at specific time intervals. Fig. 9a shows the Cs$^+$ removal rate of the

adsorbents over the contact time. The HPVA and MHPVA remove 90 % of Cs$^+$ after 5 and 3 h

contact time, and reach equilibrium after 10 and 6 h, respectively. The removal rate was

quantified using a pseudo-second order kinetic model assuming that chemisorption is the

rate-determining step [1]. The linear form of the model equation can be expressed as:

$$\frac{t}{q_t} = \frac{1}{k_2 q_e{}^2} + \frac{t}{q_e} \qquad (7)$$

where q_t is the adsorbed amount of Cs$^+$ at time t (mg/g), k_2 is the rate constant (g/mg·min), q_e

is the adsorption capacity at equilibrium (mg/g). The initial adsorption rate V_0 (mg/g·min)

was determined from the following equation:

$$V_0 = k_2 q_e{}^2 \qquad (8)$$

The parameters k_2 and q_e were determined from the slope and intercept of t/q_t versus t (Fig.

S4). As indicated in Table 5, the removal rate of the MHPVA was about 2 times faster than

that of HPVA in terms of k_2 and V_0. The faster removal rate of the MHPVA can be explained

by the higher content of K$^+$ and more surface sensitive ion exchange sites. To identify the

15

surface chemistry, XPS analysis was used as a technique to analyze surface compositional information up to 10 nm depth. The XPS spectra of the MHPVA (Fig. 5 and 9c) clearly showed the presence of K and Fe before Cs^+ adsorption, while for HPVA (Fig. 9b and Fig. S5, S6), the peaks associated with K and Fe were not distinctly identified. In addition, to confirm the participation of K^+ in Cs^+ adsorption, the MHPVA was submerged in an excess amount of 0.01 M Cs^+ solution for 24 h, and K2p and Cs3d spectra were measured. As expected, the surface K^+ was nearly exhausted (Fig. 9c) and intense Cs3d peaks (Fig. 9d, 724.6 and 738.7 eV) appeared. Considering the results, the MHPVA has a certain amount of KCuHCF near the surface which was aided by c-Fe_3O_4, and this characteristic contributed to improved Cs^+ removal kinetics. In particular, the final Cs^+ removal rate and K_d value for the MHPVA were 99.9 % and 1.18 $\times 10^6$ mL/g, respectively, demonstrating that the MHPVA can eliminate even a trace amount of Cs^+ to purify radioactive wastes.

3.6 Effects of pH and coexisted ions

pH is one of the most important factors affecting Cs^+ adsorption performance, hence the adsorption of Cs^+ by the MHPVA was evaluated under a wide pH range from 2 to 12 with 10 ppm of Cs^+ solution. From Fig. 10a, K_d was the highest at pH 8, but as the pH was varied to strongly basic or acidic regions, the performance gradually decreased. The decrease of adsorption capacities in highly acidic (pH = 2) or highly basic (pH = 12) conditions was attributed to a competition effect between H^+ and Cs^+, and slight decomposition of the KCuHCF in highly alkaline solution [1, 16, 28, 45]. However, in terms of the removal percent, all values were above 95 % in the pH range of 4 to 10, therefore validating the effective application of the MHPVA over a broad pH range.

The effect of competing cations on the adsorption of 1 ppm Cs^+ was studied using various ionic solutions. Fig. 10b represents Cs^+ removal performance of the MHPVA in the presence of 0.01 M Mg^{2+}, Ca^{2+}, Na^+, and K^+. The performance slightly deteriorated in K^+ solution, indicating more competitive adsorption due to similar hydrated radius of Cs^+ (0.329 nm) and K^+ (0.331 nm). However, in all cases, the removal rates were above 96 % and K_d values were larger than 3×10^4 mL/g, therefore demonstrating superior selective properties of the MHPVA for Cs^+. For more realistic assessment, Cs^+ adsorption was also conducted in ground water and seawater conditions, whose specific ionic concentrations and pH information are listed in Table 6. The adsorption results (Table 7) confirmed that the MHPVA not only has superior adsorption performance in DI water and ground water, but also demonstrates impressive selective properties for Cs^+ when submerged in seawater that contains competing ions which are significantly more concentrated than Cs^+ (10,000 times or more). Furthermore, both K_d and removal rates increased as the Cs^+ concentration decreased, thus highlighting that the MHPVA has a high potential to be used as an adsorbent to remediate contaminated environments of low Cs^+ concentration, below 1 ppm [16]. During these experiments, it was shown that the MHPVA was stable in both ground water and seawater conditions, and easily recovered using a magnet following 24 h contact time. Therefore, in combination with a facile and stable recovery, the high Cs^+ selective properties of the MHPVA are extremely beneficial to treat large volumes of radioactive contaminated water, which contributes to significant waste volume reduction and mitigation of any long-term environmental concerns.

4 Conclusions

In this study, KCuHCF immobilized magnetic hydrogel has been prepared by a simple freeze/thaw method to remove Cs^+ ions from contaminated environments. The MHPVA has a cross-linked macro-porous polymer structure, with c-Fe_3O_4 and KCuHCF nanoparticles dispersed throughout the hydrogel matrix. The embedded c-Fe_3O_4 particles enabled the rapid recovery of the hydrogel adsorbent from an aqueous environment. The equilibrium Cs^+ adsorption isotherms were well fitted using the Langmuir model, and the maximum Cs^+ adsorption capacity of the MHPVA was determined to be 82.8 mg/g. In the kinetics experiments (8.3 ppm Cs^+, V/m = 1000 mL/g), adsorption by the MHPVA reached equilibrium within 6 h, with almost complete Cs^+ removal of 99.9 %, along with a very high K_d value of 1.18×10^6 mL/g. The MHPVA exhibited superior removal performance compared to HPVA in terms of capacities and kinetics. The difference in the performance is related to the higher K^+ composition in the immobilized KCuHCF and surface-rich KCuHCF contents. In addition, it was shown that the MHPVA provided stable removal performance over a wide pH range, and superior removal efficiency above 96 % in the presence of excessive competing cations (0.01 M in the presence of 1 ppm Cs^+ solution). Moreover, The MHPVA showed high selectivity when submerged in low Cs^+ concentration (around 1 ppm) environments including ground water and seawater with competing cations. Following Cs^+ uptake, the MHPVA can be easily recovered by the use of magnets, producing a turbidity-free environment. Therefore, combined with a simple and economic preparation step, the synthesized MHPVA is one of the most promising adsorbents not only for the effective Cs^+ removal, but also for the facile magnetic separation.

19

References

[1] H.J. Yang, H.Y. Li, J.L. Zhai, L. Sun, Y. Zhao, H.W. Yu, Magnetic prussian blue/graphene oxide nanocomposites caged in calcium alginate microbeads for elimination of cesium ions from water and soil, Chemical Engineering Journal, 246 (2014) 10-19.

[2] S.J. Datta, W.K. Moon, D.Y. Choi, I.C. Hwang, K.B. Yoon, A Novel Vanadosilicate with Hexadeca-Coordinated Cs+ Ions as a Highly Effective Cs+ Remover, Angew Chem Int Edit, 53 (2014) 7203-7208.

[3] T. Vincent, C. Vincent, Y. Barre, Y. Guari, G. Le Saout, E. Guibal, Immobilization of metal hexacyanoferrates in chitin beads for cesium sorption: synthesis and characterization, Journal of Materials Chemistry A, 2 (2014) 10007-10021.

[4] A. Khannanov, V.V. Nekljudov, B. Gareev, A. Kiiamov, J.M. Tour, A.M. Dimiev, Oxidatively modified carbon as efficient material for removing radionuclides from water, Carbon, 115 (2017) 394-401.

[5] S.B. Yang, C. Han, X.K. Wang, M. Nagatsu, Characteristics of cesium ion sorption from aqueous solution on bentonite- and carbon nanotube-based composites, Journal of Hazardous Materials, 274 (2014) 46-52.

[6] Y. Kim, Y.K. Kim, S. Kim, D. Harbottle, J.W. Lee, Nanostructured potassium copper hexacyanoferrate-cellulose hydrogel for selective and rapid cesium adsorption, Chemical Engineering Journal, 313 (2017) 1042-1050.

[7] H.L. Chang, W.H. Shih, A general method for the conversion of fly ash into zeolites as ion exchangers for cesium, Industrial & Engineering Chemistry Research, 37 (1998) 71-78.

[8] P.K. Sinha, P.K. Panicker, R.V. Amalraj, V. Krishnasamy, Treatment of Radioactive Liquid Waste Containing Cesium by Indigenously Available Synthetic Zeolites - a Comparative-Study, Waste Manage, 15 (1995) 149-157.

[9] H.M. Liu, A. Yonezawa, K. Kumagai, M. Sano, T. Miyake, Cs and Sr removal over highly effective adsorbents ETS-1 and ETS-2, Journal of Materials Chemistry A, 3 (2015) 1562-1568.

[10] A.J. Celestian, J.D. Kubicki, J. Hanson, A. Clearfield, J.B. Parise, The Mechanism Responsible for Extraordinary Cs Ion Selectivity in Crystalline Silicotitanate, Journal of the American Chemical Society, 130 (2008) 11689-11694.

[11] A. Dyer, M. Pillinger, S. Amin, Ion exchange of caesium and strontium on a titanosilicate analogue of the mineral pharmacosiderite, Journal of Materials Chemistry, 9 (1999) 2481-2487.

[12] J.L. Mertz, Z.H. Fard, C.D. Malliakas, M.J. Manos, M.G. Kanatzidis, Selective Removal of Cs+, Sr2+, and Ni2+ by K2xMgxSn3-xS6 (x=0.5-1) (KMS-2) Relevant to Nuclear Waste Remediation, Chemistry of Materials, 25 (2013) 2116-2127.

[13] D. Sarma, C.D. Malliakas, K.S. Subrahmanyam, S.M. Islama, M.G. Kanatzidis, K2xSn4-xS8-x

(x=0.65-1): a new metal sulfide for rapid and selective removal of Cs+, Sr2+ and UO22+ ions, Chem Sci, 7 (2016) 1121-1132.

[14] M.J. Manos, M.G. Kanatzidis, Highly Efficient and Rapid Cs+ Uptake by the Layered Metal Sulfide K2xMnxSn3-xS6 (KMS-1), Journal of the American Chemical Society, 131 (2009) 6599-6607.

[15] S.B. Yang, N. Okada, M. Nagatsu, The highly effective removal of Cs+ by low turbidity chitosan-grafted magnetic bentonite, Journal of Hazardous Materials, 301 (2016) 8-16.

[16] H.J. Yang, H.Y. Li, J.L. Zhai, H.W. Yu, In situ growth of Prussian blue nanocrystal within Fe3+ crosslinking PAA resin for radiocesium highly efficient and rapid separation from water, Chemical Engineering Journal, 277 (2015) 40-47.

[17] A. Takahashi, N. Minami, H. Tanaka, K. Sue, K. Minami, D. Parajuli, K.M. Lee, S.I. Ohkoshi, M. Kurihara, T. Kawamoto, Efficient synthesis of size-controlled open-framework nanoparticles fabricated with a micro-mixer: route to the improvement of Cs adsorption performance, Green Chem, 17 (2015) 4228-4233.

[18] J. Qian, J.Q. Ma, W.W. He, D.B. Hua, Facile Synthesis of Prussian Blue Derivate-Modified Mesoporous Material via Photoinitiated Thiol-Ene Click Reaction for Cesium Adsorption, Chem-Asian J, 10 (2015) 1738-1744.

[19] C. Delchet, A. Tokarev, X. Dumail, G. Toquer, Y. Barre, Y. Guari, C. Guerin, J. Larionova, A. Grandjean, Extraction of radioactive cesium using innovative functionalized porous materials, Rsc Advances, 2 (2012) 5707-5716.

[20] R.Z. Chen, H. Tanaka, T. Kawamoto, M. Asai, C. Fukushima, M. Kurihara, M. Ishizaki, M. Watanabe, M. Arisaka, T. Nankawa, Thermodynamics and Mechanism Studies on Electrochemical Removal of Cesium Ions from Aqueous Solution Using a Nanoparticle Film of Copper Hexacyanoferrate, Acs Applied Materials & Interfaces, 5 (2013) 12984-12990.

[21] J. Causse, A. Tokarev, J. Ravaux, M. Moloney, Y. Barre, A. Grandjean, Facile one-pot synthesis of copper hexacyanoferrate nanoparticle functionalised silica monoliths for the selective entrapment of Cs-137, Journal of Materials Chemistry A, 2 (2014) 9461-9464.

[22] R. Turgis, G. Arrachart, C. Delchet, C. Rey, Y. Barre, S. Pellet-Rostaing, Y. Guari, J. Larionova, A. Grandjean, An Original "Click and Bind" Approach for Immobilizing Copper Hexacyanoferrate Nanoparticles on Mesoporous Silica, Chemistry of Materials, 25 (2013) 4447-4453.

[23] Y.K. Kim, Y. Kim, S. Kim, D. Harbottle, J.W. Lee, Solvent-assisted synthesis of potassium copper hexacyanoferrate embedded 3D-interconnected porous hydrogel for highly selective and rapid cesium ion removal, Journal of Environmental Chemical Engineering, 5 (2017) 975-986.

[24] M.A. Olatunji, M.U. Khandaker, H.N.M.E. Mahmud, Y.M. Amin, Influence of adsorption parameters on cesium uptake from aqueous solutions- a brief review, RSC Advances, 5 (2015) 71658-71683.

[25] H.-M. Yang, S.-C. Jang, S.B. Hong, K.-W. Lee, C. Roh, Y.S. Huh, B.-K. Seo, Prussian blue-functionalized magnetic nanoclusters for the removal of radioactive cesium from water, Journal of

21

Alloys and Compounds, 657 (2016) 387-393.

[26] H.X. Zhang, X. Zhao, J.Y. Wei, F.Z. Li, Removal of cesium from low-level radioactive wastewaters using magnetic potassium titanium hexacyanoferrate, Chemical Engineering Journal, 275 (2015) 262-270.

[27] R. Yi, G. Ye, F. Wu, M. Wen, X. Feng, J. Chen, Highly efficient removal of 137Cs in seawater by potassium titanium ferrocyanide functionalized magnetic microspheres with multilayer core-shell structure, RSC Advances, 4 (2014) 37600-37608.

[28] H.J. Yang, L. Sun, J.L. Zhai, H.Y. Li, Y. Zhao, H.W. Yu, In situ controllable synthesis of magnetic Prussian blue/graphene oxide nanocomposites for removal of radioactive cesium in water, Journal of Materials Chemistry A, 2 (2014) 326-332.

[29] L. Chang, S. Chang, W. Chen, W. Han, Z. Li, Z. Zhang, Y. Dai, D. Chen, Facile one-pot synthesis of magnetic Prussian blue core/shell nanoparticles for radioactive cesium removal, RSC Advances, 6 (2016) 96223-96228.

[30] C. Dwivedi, S.K. Pathak, M. Kumar, S.C. Tripathi, P.N. Bajaj, Preparation and characterization of potassium nickel hexacyanoferrate-loaded hydrogel beads for the removal of cesium ions, Environ Sci-Wat Res, 1 (2015) 153-160.

[31] M. Pasta, C.D. Wessells, N. Liu, J. Nelson, M.T. McDowell, R.A. Huggins, M.F. Toney, Y. Cui, Full open-framework batteries for stationary energy storage, Nature Communications, 5 (2014).

[32] H. Qu, D. Caruntu, H. Liu, C.J. O'Connor, Water-Dispersible Iron Oxide Magnetic Nanoparticles with Versatile Surface Functionalities, Langmuir, 27 (2011) 2271-2278.

[33] S. Liu, G.L. Pan, G.R. Li, X.P. Gao, Copper hexacyanoferrate nanoparticles as cathode material for aqueous Al-ion batteries, Journal of Materials Chemistry A, 3 (2015) 959-962.

[34] B. Jiang, W.L. Hom, X. Chen, P. Yu, L.C. Pavelka, K. Kisslinger, J.B. Parise, S.R. Bhatia, R.B. Grubbs, Magnetic Hydrogels from Alkyne/Cobalt Carbonyl-Functionalized ABA Triblock Copolymers, Journal of the American Chemical Society, 138 (2016) 4616-4625.

[35] A. Nilchi, R. Saberi, M. Moradi, H. Azizpour, R. Zarghami, Adsorption of cesium on copper hexacyanoferrate-PAN composite ion exchanger from aqueous solution, Chemical Engineering Journal, 172 (2011) 572-580.

[36] C. Dwivedi, A. Kumar, K.K. Singh, A.K. Juby, M. Kumar, P.K. Wattal, P.N. Bajaj, Copper hexacyanoferrate-polymer composite beads for cesium ion removal: Synthesis, characterization, sorption, and kinetic studies, J Appl Polym Sci, 129 (2013) 152-160.

[37] A. Singhal, M. Kaur, K.A. Dubey, Y.K. Bhardwaj, D. Jain, C.G.S. Pillai, A.K. Tyagi, Polyvinyl alcohol-In2O3 nanocomposite films: synthesis, characterization and gas sensing properties, RSC Advances, 2 (2012) 7180-7189.

[38] A. Pourjavadi, B. Pourbadiei, M. Doroudian, S. Azari, Preparation of PVA nanocomposites using salep-reduced graphene oxide with enhanced mechanical and biological properties, RSC Advances, 5 (2015) 92428-92437.

[39] X. Wang, Q. Xiang, B. Liu, L. Wang, T. Luo, D. Chen, G. Shen, TiO2 modified FeS Nanostructures with Enhanced Electrochemical Performance for Lithium-Ion Batteries, Sci Rep-Uk, 3 (2013) 2007.

[40] X. Wei, Y. Zhou, Y. Li, W. Shen, Polymorphous transformation of rod-shaped iron oxides and their catalytic properties in selective reduction of NO by NH3, RSC Advances, 5 (2015) 66141-66146.

[41] Y. Yang, H.J. Gao, L.Q. Zheng, Anhydrous proton exchange membranes at elevated temperatures: effect of protic ionic liquids and crosslinker on proton conductivity, Rsc Advances, 5 (2015) 17683-17689.

[42] M. Ishizaki, S. Akiba, A. Ohtani, Y. Hoshi, K. Ono, M. Matsuba, T. Togashi, K. Kananizuka, M. Sakamoto, A. Takahashi, T. Kawamoto, H. Tanaka, M. Watanabe, M. Arisaka, T. Nankawa, M. Kurihara, Proton-exchange mechanism of specific Cs+ adsorption via lattice defect sites of Prussian blue filled with coordination and crystallization water molecules, Dalton T, 42 (2013) 16049-16055.

[43] S.C. Jang, Y. Haldorai, G.W. Lee, S.K. Hwang, Y.K. Han, C. Roh, Y.S. Huh, Porous three-dimensional graphene foam/Prussian blue composite for efficient removal of radioactive Cs-137, Sci Rep-Uk, 5 (2015).

[44] T. Vincent, C. Vincent, E. Guibal, Immobilization of Metal Hexacyanoferrate Ion-Exchangers for the Synthesis of Metal Ion Sorbents-A Mini-Review, Molecules, 20 (2015) 20582-20613.

[45] R.Z. Chen, H. Tanaka, T. Kawamoto, M. Asai, C. Fukushima, H.T. Na, M. Kurihara, M. Watanabe, M. Arisaka, T. Nankawa, Selective removal of cesium ions from wastewater using copper hexacyanoferrate nanofilms in an electrochemical system, Electrochim Acta, 87 (2013) 119-125.
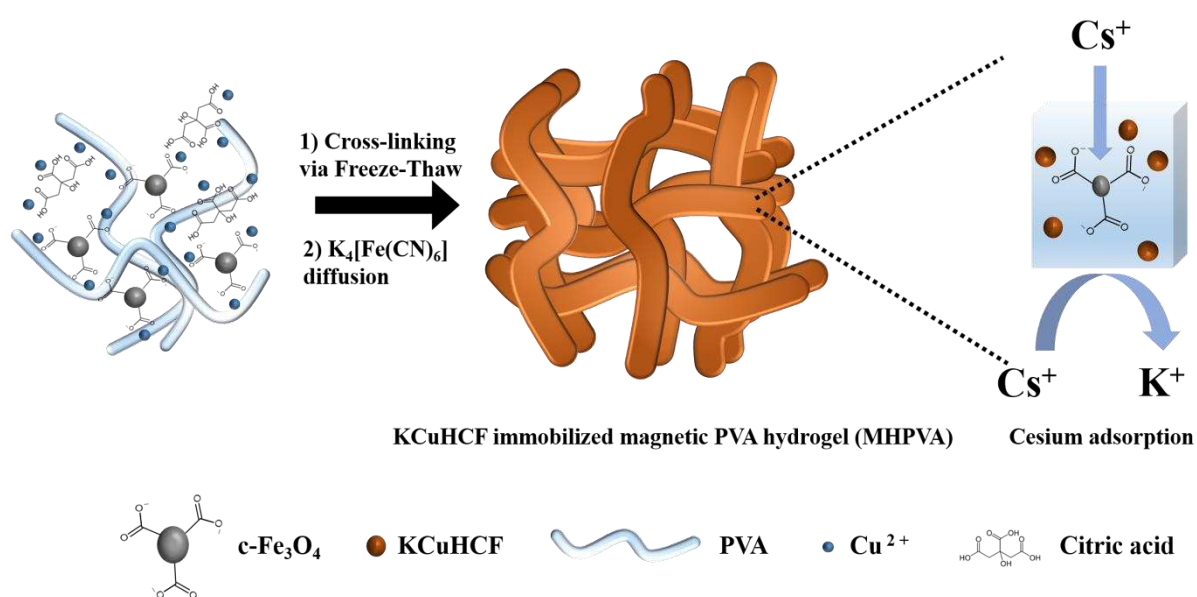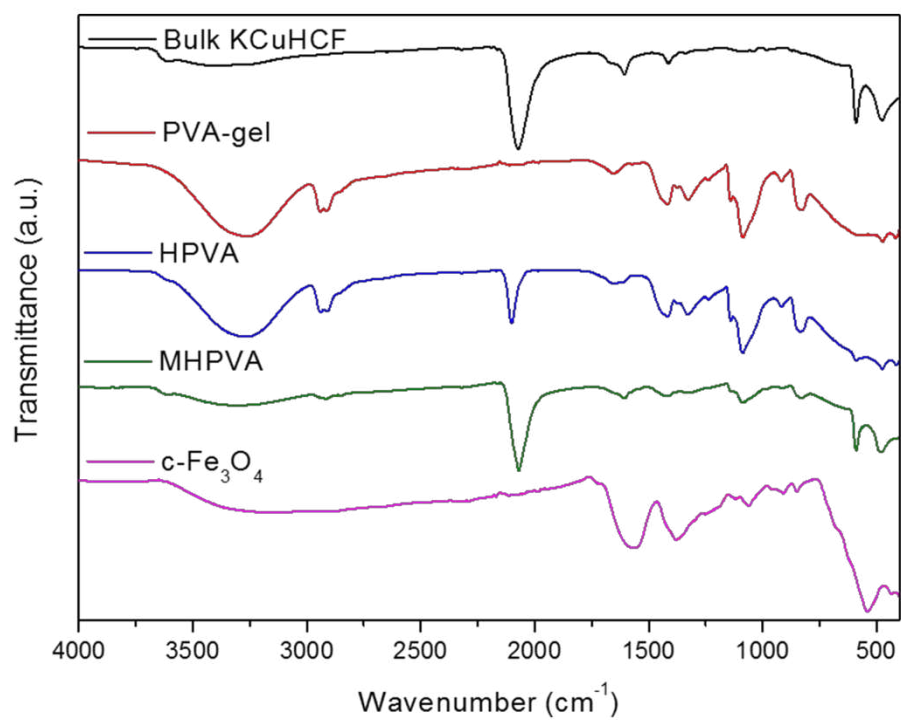
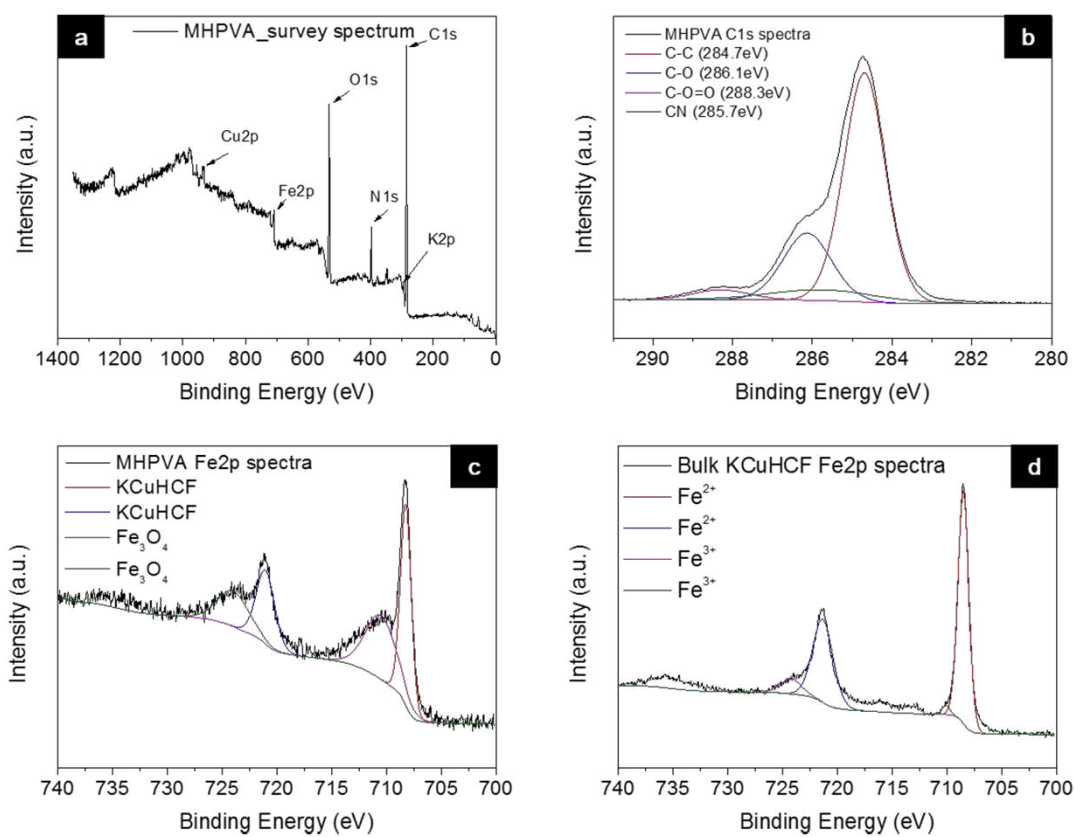**Fig. 1. Schematic representation for MHPVA synthesis and subsequent Cs$^+$ adsorption.**
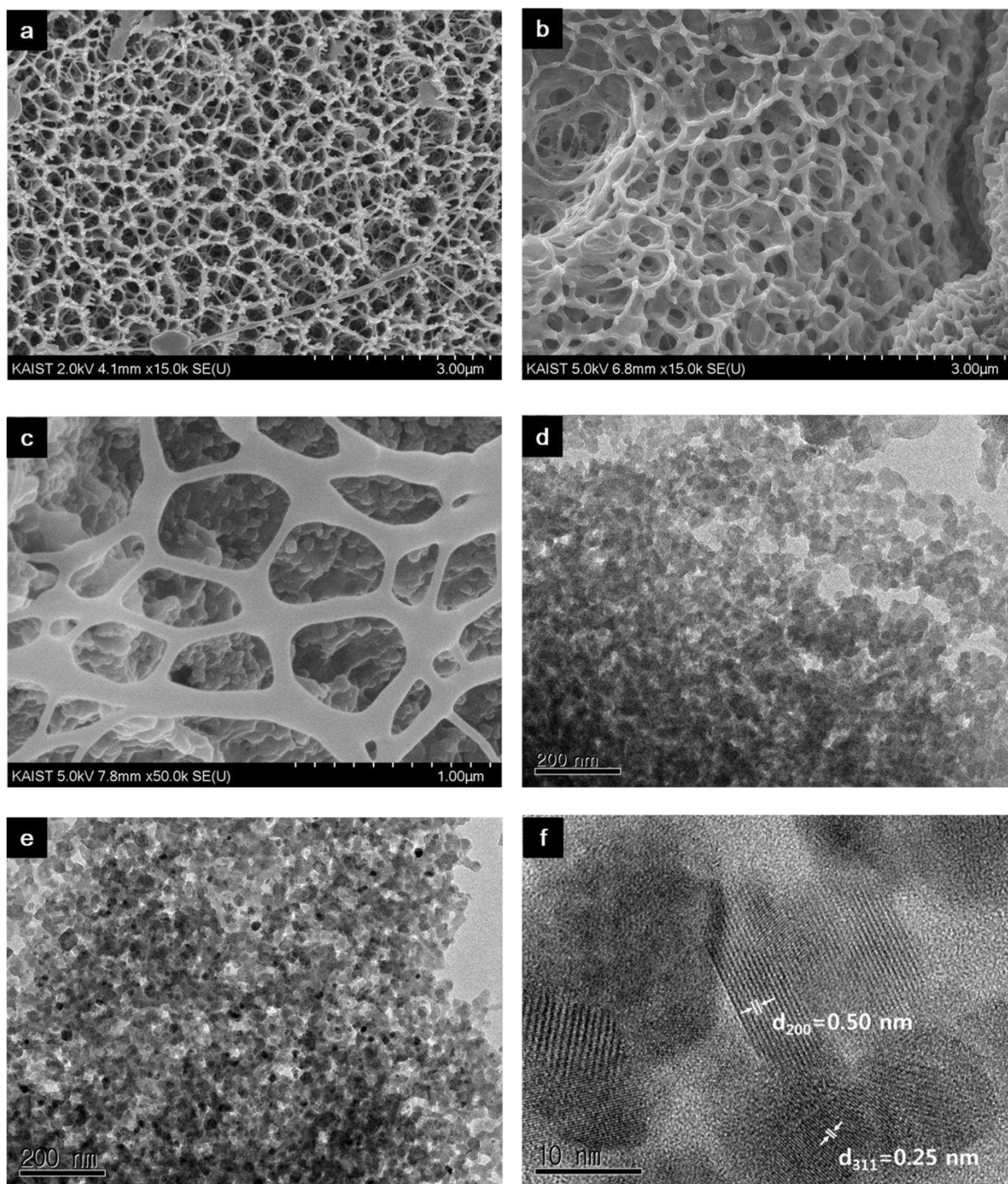
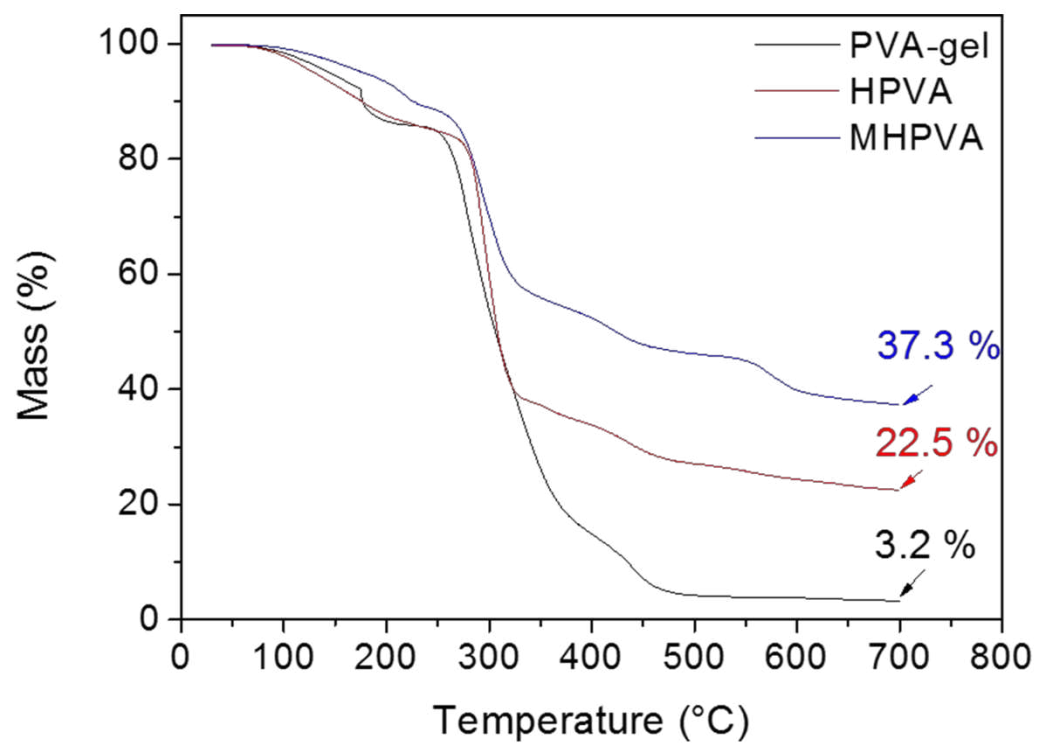**Fig. 2. SEM images of (a) PVA-gel and (b), (c) MHPVA. TEM images of (d) HPVA and (e), (f) MHPVA.**
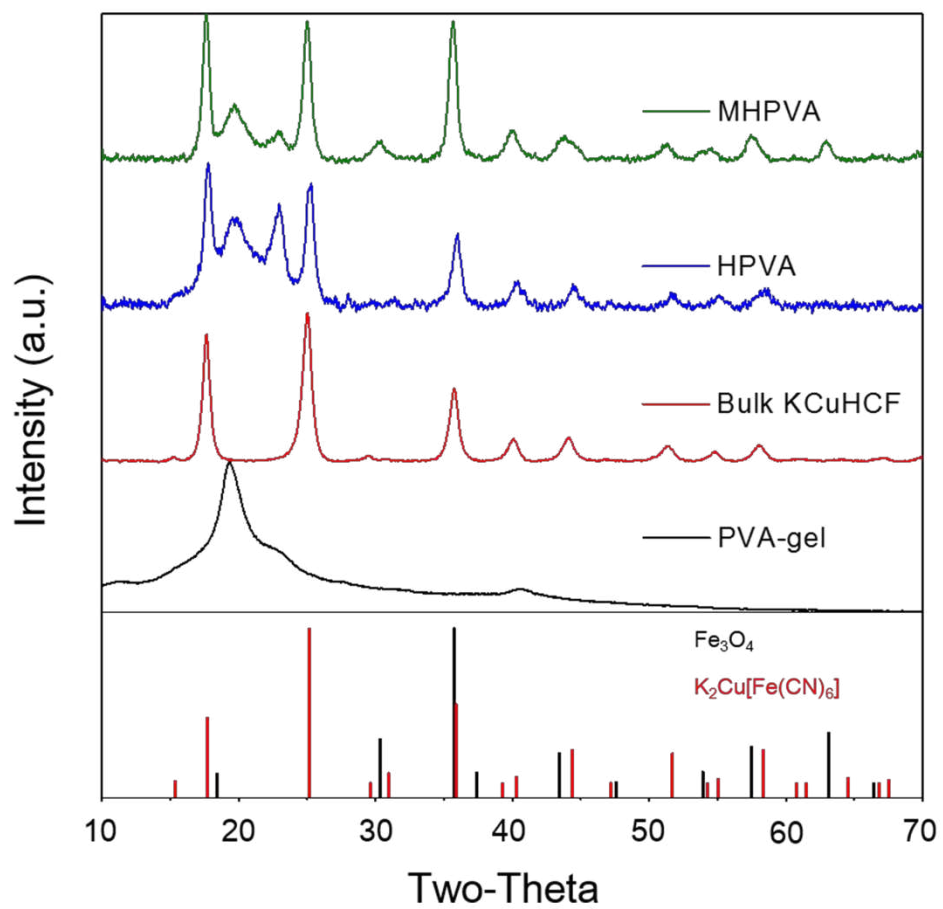
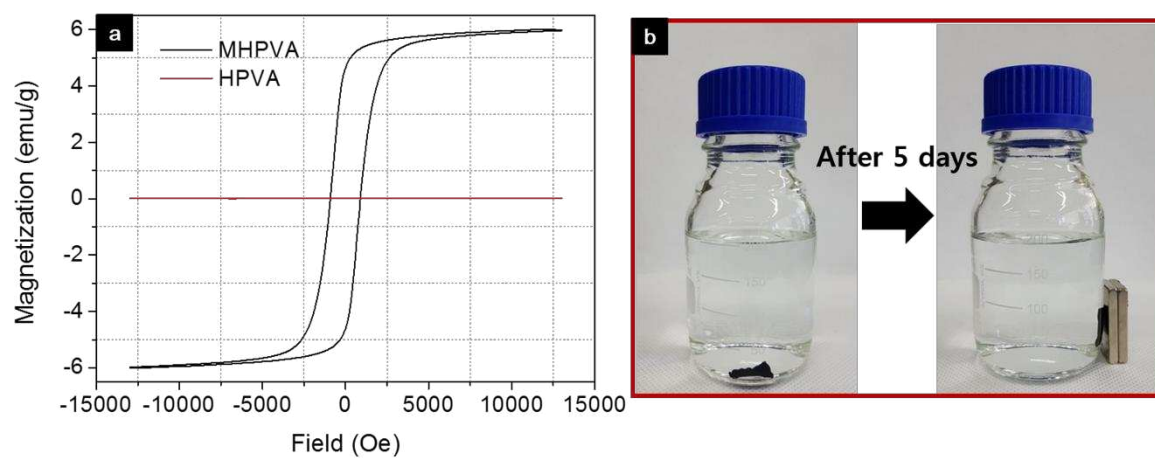**Fig. 3. XRD patterns for PVA-gel, bulk KCuHCF, HPVA and MHPVA.**

Fig. 4. FTIR spectra for bulk KCuHCF, PVA-gel, HPVA, MHPVA and c-Fe₃O₄.

27

Fig. 5. XPS (a) survey spectra (b) C1s spectra (c) Fe2p spectra for MHPVA, and (d) Fe2p spectra for bulk KCuHCF.
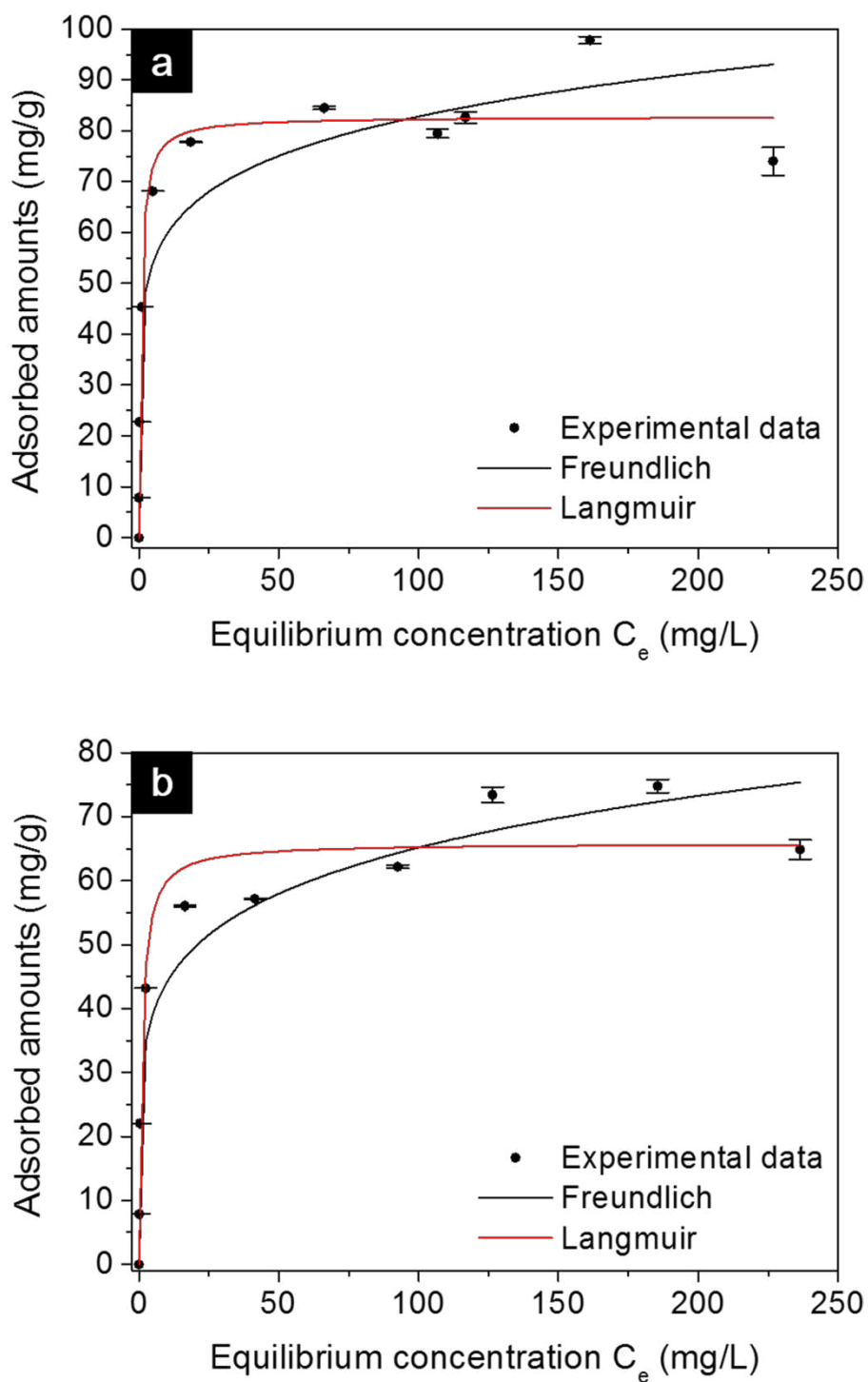
Fig. 6. TGA profile curves of PVA-gel, HPVA, and MHPVA.
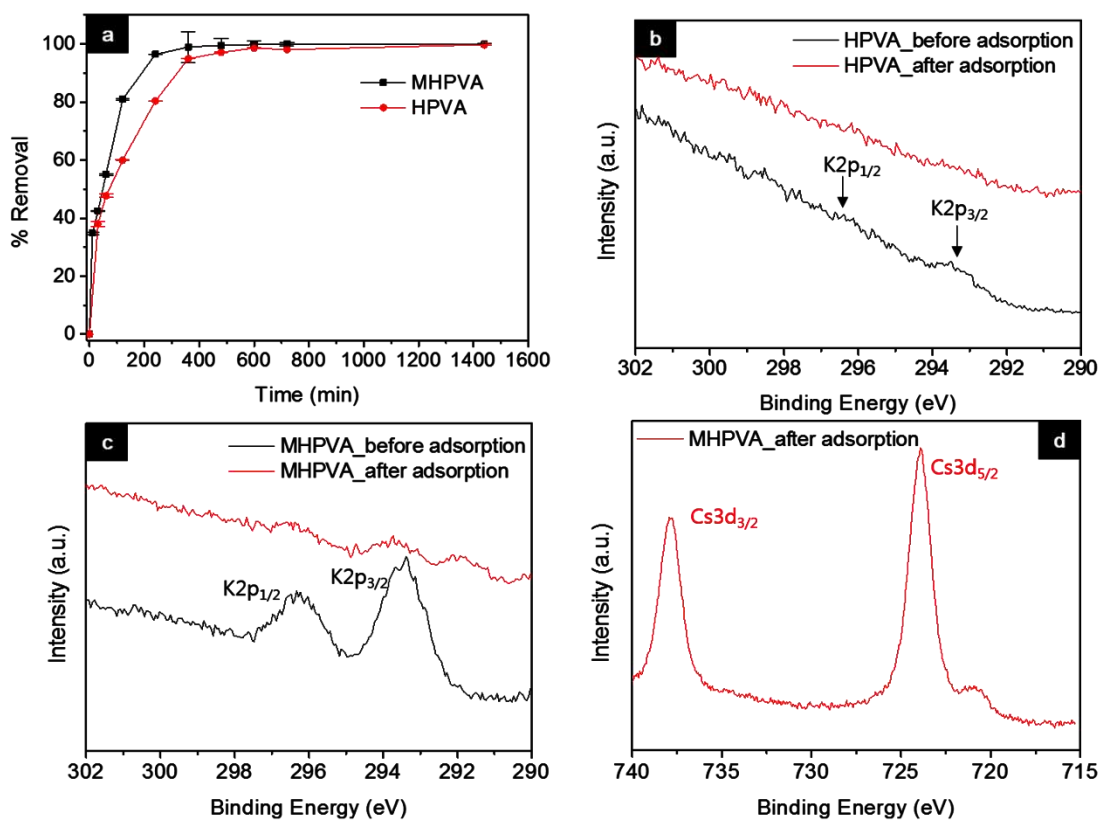
Fig. 7. (a) Field-dependent magnetization curve of HPVA and MHPVA. (b) macroscopic pictures for magnetic separation of MHPVA.

Fig. 8. Cs$^+$ adsorption isotherms for (a) MHPVA and (b) HPVA with Freundlich and Langmuir fitting curves.

31

Fig. 9. (a) Cs⁺ removal kinetics of HPVA and MHPVA. **XPS K2p spectra for (b) HPVA and (c) MHPVA. XPS (d) Cs3d spectra of MHPVA.**
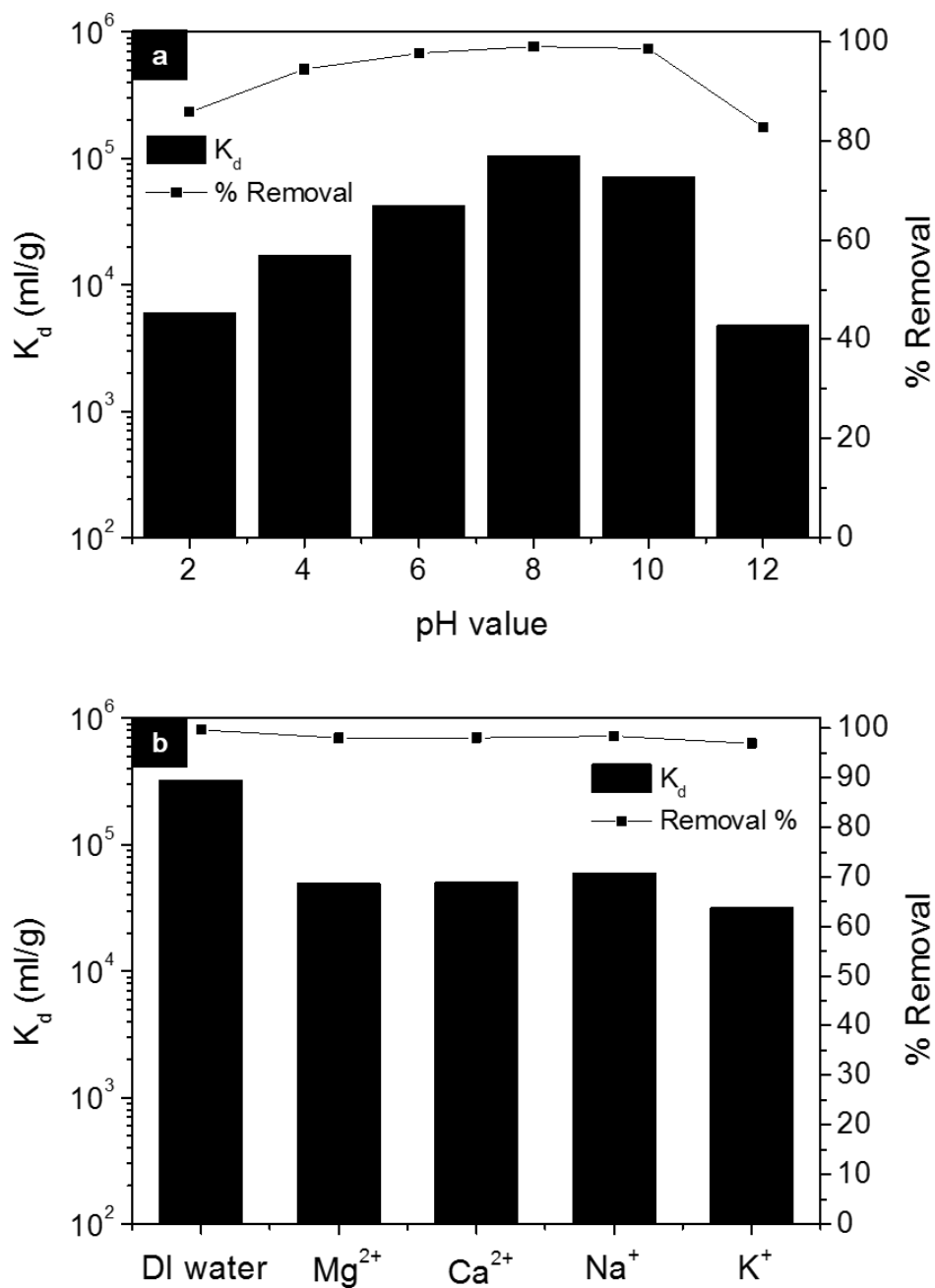
Fig. 10. (a) Effect of initial solution pH ($C_{0,\,Cs+} \approx$ 10ppm) and (b) the effect of different competitive cations ($C_{0,\,Cs+} \approx$ 1 ppm) for Cs^+ adsorption by MHPVA.

Table 1 ICP-OES elemental analyses of HPVA and MHPVA.

Sample	ICP-OES (wt %)			K/Cu	Fe(HCF)/Cu[a]	Chemical composition	KCuHCF (wt %)
	Cu	Fe	K				
HPVA	5.95	3.30	1.61	0.44	0.63	$K_{0.44}Cu[Fe(CN)_6]_{0.63}$	20.1
MHPVA	4.04	9.12	3.70	1.48	0.87	$K_{1.48}Cu[Fe(CN)_6]_{0.87}$	19.5

[a] Fe(HCF) indicates Fe in the KCuHCF.

Table 2 Fe and Cu concentration in MHPVA immersed solution during a contact time of 5 days.

	DI water	1 day	2 day	3 day	5 day
Fe (ppm)	0.000	0.011	0.025	0.039	0.073
Cu (ppm)	0.000	0.016	0.021	0.023	0.022

Table 3 Langmuir and Freundlich isotherm constants of HPVA and MHPVA.

	Langmuir			Freundlich		
	Q_m (mg/g)	b (L/mg)	R^2	n	K_F (mg/g)	R^2
HPVA	65.9	1.00	0.95	5.92	29.96	0.92
MHPVA	82.8	1.49	0.95	7.03	43.05	0.88

Table 4 Comparison of Cs$^+$ adsorption capacities for various adsorbents.

	Capacity (mg/g)	Reference
PFMw	40.77	[1]
PB-MNC-3	45.87	[25]
M-PTH	80	[26]
KTiFC	42.23	[27]
PB/Fe$_3$O$_4$/GO	55.55	[28]
MPB-1	145.8	[29]
MHPVA	82.8	This work

Table 5 Pseudo-second order kinetic model parameters for HPVA and MHPVA.

	q_e (mg/g)	k_2 (g/mg min)	V_0 (mg/g min)	R^2
HPVA	8.448	0.0020	0.141	0.99
MHPVA	8.455	0.0043	0.309	0.99

Table 6 Concentration of major cations and pH value in simulated groundwater and seawater.

Water type	Na$^+$ (ppm)	K$^+$ (ppm)	Mg^{2+} (ppm)	Ca^{2+} (ppm)	pH value
Groundwater	117	180	116	15	8.59
Seawater	10409	359	1327	176	7.95

Table 7 Removal efficiency (%) and K_d value for MHPVA in DI water, groundwater and seawater.

	Initial Cs^+ (ppm)	Removal (%)	K_d (ml/g)
DI water	10.5	99.1	1×10^5
	1.0	99.7	3.2×10^5
Groundwater	10.6	92.9	1.3×10^4
	1.2	94.5	1.7×10^4
Seawater	13.4	84.0	5.2×10^3
	1.4	92.9	1.3×10^4